Stochastic Unit Commitment with High-penetration Offshore Wind Power Generation in Typhoon Scenarios

Yanqi Liu, Dundun Liu, *Member*, *IEEE*, and Hongcai Zhang, *Senior Member*, *IEEE*

***Abstract*—To tackle the energy crisis and climate change, wind farms are being heavily invested in across the world. In China's coastal areas, there are abundant wind resources and numerous offshore wind farms are being constructed. The secure operation of these wind farms may suffer from typhoons, and researchers have studied power system operation and resilience enhancement in typhoon scenarios. However, the intricate movement of a typhoon makes it challenging to evaluate its spatial-temporal impacts. Most published papers only consider predefined typhoon trajectories neglecting uncertainties. To address this challenge, this study proposes a stochastic unit commitment model that incorporates high-penetration offshore wind power generation in typhoon scenarios. It adopts a data-driven method to describe the uncertainties of typhoon trajectories and considers the realistic anti-typhoon mode in offshore wind farms. A two-stage stochastic unit commitment model is designed to enhance power system resilience in typhoon scenarios. We formulate the model into a mixed-integer linear programming problem and then solve it based on the computationally-efficient progressive hedging algorithm (PHA). Finally, numerical experiments validate the effectiveness of the proposed method.**

***Index Terms*—Unit commitment, two-stage stochastic programming, offshore wind farm, typhoon.**

I. Introduction

CHINA announced its plan to achieve peak carbon emission by 2030 and be carbon neutral by 2060 at the United Nations General Assembly in September 2020 [1]. This target is highly challenging because its current power system is dominated by fossil fuel generation [2]. To meet this target, China has made substantial investments in renewable generation. Offshore wind power is a particularly environmentally friendly form of renewable generation and has remarkable advantages compared with the onshore one. The South China coast possesses abundant offshore wind resources, and the planned installed capacity for offshore wind power is expected to reach 30 million kW in 2030, accounting for 15% of the total installed capacity in Guangdong Province, as outlined in the Guangdong Provincial Maritime Development Plan (2017-2030) of China. However, the integration of high-penetration wind power generation presents significant challenges to power system operation due to the stochastic and intermittent nature of wind [3], [4]. Unit commitment (UC) is a crucial problem in day-ahead power system operations that involves determining unit status and power generation, and it is affected by the uncertainty and variability of wind power [5]. Scholars have employed various methods such as stochastic programming [6], robust optimization [7], and chance-constrained optimization [8] to handle this uncertainty. While accurately predicting wind generation during daily operations is challenging, operators face even greater difficulties during extreme weather events.

Southeast China is a highly susceptible region to tropical cyclones [9], and Guangdong Province experiences the highest number of typhoon landings [10]. Some published papers have studied the UC problem in typhoon scenarios to reduce load shedding, renewable generation curtailment, and operational costs and enhance power system reliability. For example, [11] proposes a security-constrained UC model that incorporates the estimation of transmission tower failures. Reference [12] considers grid hardening techniques to minimize the hardening investment and load loss in typhoon scenarios. Reference [13] utilizes emergency demand response programs to improve system resilience. Reference [14] introduces two penalty terms to improve the homogeneity of the flow distribution and loading rates of power lines in typhoon scenarios. Reference [15] employs a predefined typhoon track to assess potentially affected power lines. These papers provide various instructive methods to model the transmission line and tower failures in typhoon scenarios, while the impacts of typhoons on offshore wind farms are not addressed. Offshore wind farms may be compelled to cease operations for protection or may even sustain damage in extreme wind scenarios during typhoons [16]. This can result in abrupt power generation losses and threaten the security

Manuscript received: January 14, 2023; revised: May 11, 2023; accepted: July 6, 2023. Date of CrossCheck: July 6, 2023. Date of online publication: August 16, 2023.

This paper was supported in part by the Science and Technology Development Fund, Macau SAR (No. SKL-IOTSC(UM)-2021-2023, 0003/2020/AKP).

Y. Liu and H. Zhang (corresponding author) are with the State Key Laboratory of Internet of Things for Smart City and Department of Electrical and Computer Engineering, University of Macau, Macao 999078, China (e-mail: liu.yanqi@connect.um.edu.mo; hczhang@um.edu.mo).

D. Liu is with the University of Macau Zhuhai UM Science and Technology Research Institute, Zhuhai, China (e-mail: zumri.dundunliu@um.edu.mo).

DOI: 10.35833/MPCE.2023.000019

of power systems. Hence, it is essential to investigate the strategic operation of power systems with high-penetration offshore wind power generation in typhoon scenarios.

Analyzing the influence of typhoons on a power system is technically challenging due to the complex weather mechanisms involved in their generation, evolution, and disappearance. Many published papers have explored the impacts of typhoons on power systems. For example, the wind power ramping of an offshore wind farm is optimized based on a predetermined typhoon path in [17]. Reference [12] considers grid hardening techniques, and minimizes the hardening investment and load shedding under various typhoon categories and paths. Robust optimization is used to account for a multi-zone-based uncertainty set along the typhoon path in [18]. Similarly, [19] constructs a data-driven uncertainty set of the affected components with an estimated typhoon track. Though the abovementioned papers have made remarkable research advancements, there are still notable research gaps to fill. For example, [17] only considers a predefined typhoon path disregarding the randomness of its trajectory and stochastic impacts. Some papers utilize different typhoon categories to evaluate vulnerable distribution lines [12], [20], which is not a suitable approach for the day-ahead strategy. Some other papers divide the power system into distinct regions based on expert assessments and assume the electrical components are uniformly affected by a typhoon [18], [19].

The impacts of typhoons on offshore wind farms and power systems are closely tied to their spatial-temporal characteristics. Meteorologists have conducted studies on the formulation, evolution, and dissipation of typhoon disasters [21] and have developed new schemes for prediction, prevention, and mitigation [22]. A typhoon simulation model, incorporating the time-varying wind field and motion path proposed in [23], has been widely utilized to describe the spatial-temporal characteristics and assess the impacts on power systems [24]. However, the prediction errors of this typhoon model accumulate over time and become non-negligible in the day-ahead UC problem. To address this uncertainty, [25] employs stochastic programming, which can be computationally demanding when dealing with a large number of typhoon scenarios.

As mentioned above, the impacts of typhoons on a power system with high-penetration offshore wind power generation have not been fully studied. The stochastic nature of typhoon tracks plays a significant role in wind farm and power system operations, and the uncertainties need to be carefully modeled. Extensive research is required to understand the operational characteristics of offshore wind farms under impacts of typhoons. To bridge these gaps, this paper contributes by introducing a novel stochastic two-stage UC model. Based on an empirical typhoon track model, uncertain typhoon tracks are generated using the Monte Carlo sampling method. The stochastic tracks and wind field of a typhoon are incorporated to accurately describe the spatial-temporal impacts of typhoons. The operational features of an offshore wind farm, including the anti-typhoon mode and abrupt wind power generation changes, are also considered. The proposed UC model is formulated into a two-stage mixed-integer linear programming (MILP) problem that can be solved by the progressive hedging algorithm (PHA) effectively.

The remaining contents of this paper are organized as follows. In Section II, we introduce the models of typhoons and offshore wind farms. Section III presents the stochastic UC model to minimize operational costs and load shedding in typhoon scenarios. In Section IV, numerical experiments are discussed. Finally, we conclude our work in Section V.

II. Models of Typhoons and Offshore Wind Farms

This section introduces the models for typhoons and offshore wind farms. Firstly, an empirical track model is used to describe the forecasted track of an upcoming typhoon. The uncertainties associated with the typhoon track are discussed, and a Monte Carlo simulation is employed to generate typhoon scenarios. Subsequently, a typhoon wind field model is presented to obtain the wind speeds at different locations. In the offshore wind farm model, the wind speed power curve and the anti-typhoon mode are described.

A. Typhoon Model

To evaluate impacts of typhoons on offshore wind farms, the typhoon track model and the track uncertainties are discussed in this subsection. Furthermore, a time-varying wind field is developed along the typhoon track.

1) Typhoon Track Model

In day-ahead planning, power system operators will usually receive early warnings of ongoing typhoon activity, and a forecasted typhoon track is often provided by the meteorological department. The system operator shall use this typhoon information to evaluate its impacts on offshore wind farms and the power system and then propose operation strategies. In this paper, we adopt an empirical typhoon track model to describe typhoon tracks on the sea following [26]. The changes of the translation speed c and heading direction θ (in degree from the north) of a typhoon eye with time index t, i.e., $c(t)$ and $\theta(t)$, are calculated as:

$$\ln c(t+1)-\ln c(t)=a_1+a_2\psi(t)+a_3\lambda(t)+a_4\ln c(t)+a_5\theta(t)+\varepsilon_c \quad (1)$$

$$\theta(t+1)-\theta(t)=b_1+b_2\psi(t)+b_3\lambda(t)+b_4c(t)+b_5\theta(t)+b_6\theta(t-1)+\varepsilon_\theta \quad (2)$$

where ψ and λ are the latitude and longitude of the typhoon eye, respectively; ε_c and ε_θ are the residual terms following Gaussian distributions with mean values equal to zero; and the parameters a_1-a_5 and b_1-b_6 are the fitting coefficients for each $5°\times5°$ grid in the sea. Different sets of coefficients corresponding to these $5°\times5°$ grids are used for higher fitting accuracy. Similarly, the relative intensity I related to sea surface temperature at time t is calculated as:

$$\begin{aligned}\ln I(t+1)=d_1+d_2\ln I(t)+d_3\ln I(t-1)+d_4\ln I(t-2)+\\ d_5S_t(t)+d_6(S_t(t+1)-S_t(t))+\varepsilon_I\end{aligned} \quad (3)$$

where $S_t(t)$ is the sea surface temperature at time t; d_1-d_6 are the model coefficients corresponding to each $5°\times5°$ grid in the sea; and ε_I is the residual. To estimate the coefficients in (1)-(3), we utilize the least square fitting based on historical typhoon data recorded in every 6-hour interval ($\Delta T=6$

hours), which are collected from the Tropical Cyclone Center of the China Meteorological Administration [27].

2) Typhoon Track Uncertainties

When utilizing the abovementioned empirical typhoon track model for day-ahead typhoon prediction, it is inevitable to encounter prediction errors. These errors affecting both the translation speed and heading direction gradually accumulate over time, resulting in increased uncertainties in the typhoon track. There are also other sources of uncertainties besides uncertain typhoon tracks, such as sea surface temperature [26] and central pressure deficit [23]. To simplify the model, we focus solely on the uncertainties arising from the prediction errors in the typhoon track. These uncertainties contribute to discrepancies between the actual output of offshore wind farms and their forecasted values. Figure 1 shows that the wind power generation scenarios become gradually more dispersed in space as time progresses. To deal with the uncertainties induced by uncertain typhoon tracks, we generate various typhoon track scenarios and propose a stochastic UC model.

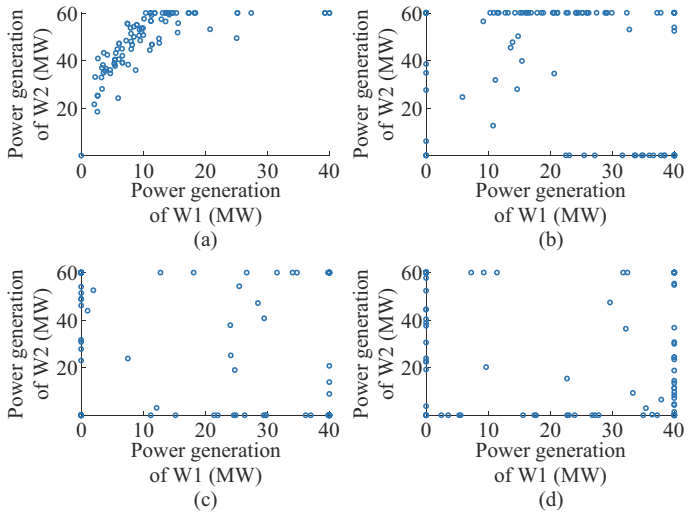

Fig. 1. Wind power generation of two offshore wind farms W1 and W2. (a) $t=6$ hours. (b) $t=12$ hours. (c) $t=18$ hours. (d) $t=24$ hours.

Here, we assume that the typhoon prediction errors follow Gaussian distributions with a zero mean, and possible typhoon tracks are centered on the forecasted track. Then, we introduce the modeling and sampling of the stochastic typhoon track.

The uncertainty associated with the typhoon track is determined based on the deviations between the empirical track and the actual historical track. To further elaborate on this, we compare the empirical track (also referred to the forecasted track) with the real historical track, as shown in Fig. 2. First, two adjacent typhoon locations, A and C, are selected from a historical track, and the empirical track model given by (1) and (2) is used to calculate the forecasted track A to B. The translation speed and heading direction can be directly obtained from the coordinates of two locations. Second, the differences, i.e., prediction errors of the translation speed and heading direction (denoted by $\Delta c=\Delta s/\Delta T$ and $\Delta\theta$, respectively), between the forecasted track A to B and the historical track A to C are calculated. Third, the abovementioned two steps are repeated for every historical track, and all the corresponding Δc and $\Delta\theta$ are collected to form two sets $\mathcal{I}^c$ and $\mathcal{I}^\theta$ of the prediction errors, respectively, as shown in Figs. 3 and 4.

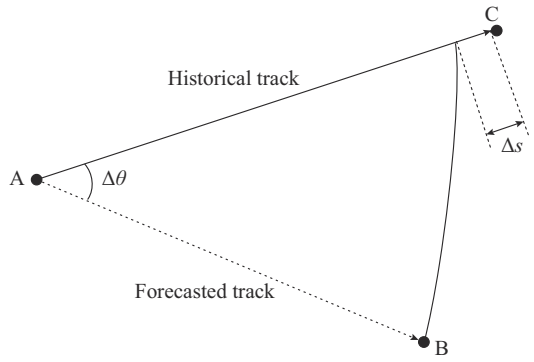

Fig. 2. Prediction error of a simulated typhoon.

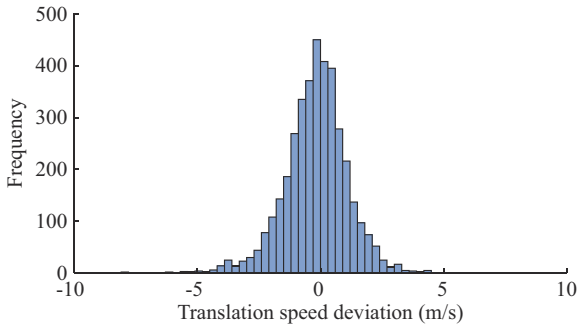

Fig. 3. Frequency distribution plot of translation speed deviations.

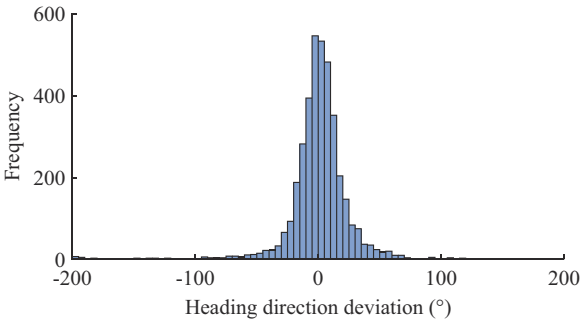

Fig. 4. Frequency distribution plot of heading direction deviations.

Then, we generate typhoon track scenarios by sequentially adding sampled prediction errors to the forecasted values using the Monte Carlo sampling. To illustrate this, we will explain the process of generating one typhoon scenario as an example. Generating additional scenarios follows a similar procedure.

Step 1: obtain the current latitude, longitude, translation speed, and heading direction of the typhoon that we are interested in.

Step 2: based on the typhoon motion information in the previous time step, calculate the translation speed c_0 and heading direction θ_0 in the next time step using the empirical typhoon track model, i.e., (1) and (2).

Step 3: sample two residual errors c_r and θ_r from the trans-

lation speed and heading direction deviation sets, $\mathcal{I}^c$ and $\mathcal{I}^\theta$, respectively.

Step 4: obtain the simulated translation speed $c_s = c_0 + c_r$ and heading direction $\theta_s = \theta_0 + \theta_r$ of the typhoon and calculate the typhoon center coordinates based on typhoon motion c_s and θ_s.

Step 5: go to *Step 2* and simulate the next typhoon location based on the current latitude, longitude, and motion in *Step 4*.

Step 6: repeat *Steps 2-5* until the last time period and obtain a complete simulated typhoon scenario.

In general, selecting a reasonable number of scenarios in the stochastic UC model involves a trade-off between model accuracy and computational efficiency. It is pointed out in [28] that Monte Carlo simulation based approximation of a stochastic programming provides an exact optimal solution with probability 1 by using the theory of large deviations and could be very efficient with a small number of scenarios to find an optimal solution. Alexander Shapiro argues that two-stage stochastic programming can be solved with reasonable accuracy using Monte Carlo sampling in [29].

First, based on previous (or initial) typhoon motion, the forecasted speed and direction are calculated based on (1) and (2) in the next time interval. Second, sampled prediction errors are added from $\mathcal{I}^\theta$ and $\mathcal{I}^c$ to the forecasted translation speed and direction, yielding a typhoon location in the next time interval. Third, the abovementioned two steps are repeated at each future scheduling moment to generate a typhoon scenario.

3) Typhoon Wind Field Model

Based on the forecasted typhoon tracks in the previous part, this part adopts a typhoon wind field model [30] to estimate wind speeds at offshore wind farms. The typhoon wind field can be described as a vortex with concentric field contour lines. The wind speed w_{sp} at a specific location is a function of its distance d to the typhoon center, which can be calculated as:

$$w_{sp} = \begin{cases} KW_m(1-\exp(-\alpha d)) & 0 \le d \le r_{mw} \\ W_m \exp\left(-\dfrac{d-r_{mw}}{r_s - r_{mw}} \ln \beta\right) & r_{mw} < d \le r_s \\ 0 & r_s < d \end{cases} \tag{4}$$

$$\alpha = \frac{1}{r_{mw}} \ln \frac{K}{K-1} \tag{5}$$

where W_m is the maximum wind speed; K is the typhoon speed parameter, which is set to be 1.14 in this paper; β is the boundary parameter, which is set to be 10 in this paper; r_{mw} is the radius to the maximum wind; and r_s is the boundary of the typhoon influence where the wind speed has reduced to W_m/β. The estimates of the time-varying parameters r_{mw} and W_m are as follows [30]:

$$\ln r_{mw} = 2.636 - 0.0005086\Delta p^2 + 0.0394899\psi \tag{6}$$

$$B = 1.38 + 0.00184\Delta p - 0.00309 r_{mw} \tag{7}$$

$$W_m = \sqrt{(B\Delta p)/(e\rho)} \tag{8}$$

where B is the Holland pressure parameter; ρ is the density of air; and Δp is the central pressure difference, which is related to the relative intensity $I(t)$, as shown in (9).

$$I(t) = \frac{\Delta p}{p_{da} - p_{dc}} \tag{9}$$

where p_{da} is the surface value of the partial pressure of ambient dry air; and p_{dc} is the minimum sustainable surface value of the central pressure for a typhoon.

B. Offshore Wind Farm Model

The wind field of a typhoon plays a crucial role in determining the impact on an offshore wind farm, thereby affecting wind power generation. Along a typhoon track, the wind speed at the offshore wind farm site depends on its distance to the typhoon eye, denoted by d, which is calculated as:

$$d = \sqrt{(\lambda_w - \lambda(t))^2 + (\psi_w - \psi(t))^2} \tag{10}$$

where $(\lambda(t), \psi(t))$ is the typhoon eye location; and (λ_w, ψ_w) is the location of the offshore wind farm. Then, the wind speed is calculated from the typhoon wind field model in (4).

The offshore wind farm generation P_w relies on the wind speed-power curve shown in Fig. 5.

$$P_w = \begin{cases} 0 & w_{sp} \le w_{ci} \text{ or } w_{sp} \ge w_{co} \\ P_r \dfrac{w_{sp} - w_{ci}}{w_r - w_{ci}} & w_{ci} < w_{sp} \le w_r \\ P_r & w_r < w_{sp} < w_{co} \end{cases} \tag{11}$$

where w_{ci}, w_{co}, and w_r are the cut-in, cut-off, and rated wind speeds, respectively; and P_r is the rated output of the offshore wind farm. In this paper, the cut-in, cut-off, and rated wind speeds are set to be 3, 12, and 20 m/s, respectively.

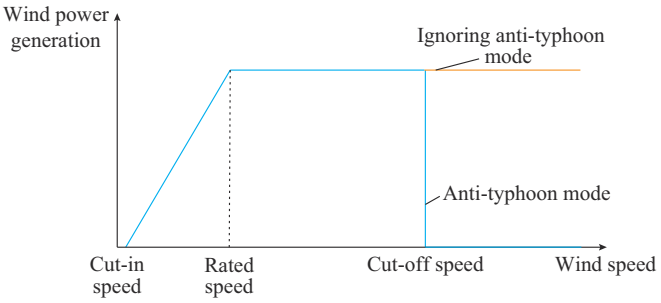

Fig. 5. Wind speed-power curve.

The wind farm is cut off under high wind speeds, resulting in tremendous power changes, which is called the anti-typhoon mode in this paper. Ignoring the realistic anti-typhoon mode can result in significant discrepancies between the day-ahead wind forecast and the actual wind conditions, posing substantial operational risks in real-time power dispatch.

III. Stochastic UC Model in Typhoon Scenarios

To account for the volatility of wind power generation in typhoon scenarios, the two-stage stochastic UC model addresses uncertainties via a number of scenarios [25]. Its first stage determines the unit status, and the second stage simulates the intraday power dispatch in each scenario. However,

solving this model can become computationally expensive if the number of scenarios is large. In this paper, we propose a two-stage stochastic UC model in typhoon scenarios and adopt a PHA to solve it efficiently.

A. Objective Function

The objective function contains the sum of the first-stage costs and the expected second-stage costs. The first-stage costs include the startup cost C_{it}^{SU}, shutdown cost C_{it}^{SD}, spinning reserve cost of the conventional generator C_{it}^{GR}, and demand-side reserve cost C_{it}^{DR} at bus i and time t. The second-stage costs are the expected intraday power scheduling costs in different typhoon scenarios, which include the operational cost C_{its}^{OP}, real-time deployed (denoted by superscript "rt") spinning reserve cost of the conventional generator C_{its}^{Grt}, demand-side reserve cost C_{its}^{Drt}, and load shedding cost C_{its}^{LS} at bus i and time t in scenario s. The probability of scenario s is π_s. The objective function is formulated as follows:

$$\min\left\{\sum_t\sum_{i\in\mathcal{I}^{\mathrm{G}}}(C_{it}^{\mathrm{SU}}+C_{it}^{\mathrm{SD}}+C_{it}^{\mathrm{GR}})+\sum_t\sum_{i\in\mathcal{I}^{\mathrm{D}}}C_{it}^{\mathrm{DR}}+\sum_s\pi_s\sum_t\left[\sum_{i\in\mathcal{I}^{\mathrm{G}}}(C_{its}^{\mathrm{OP}}+C_{its}^{\mathrm{Grt}})+\sum_{i\in\mathcal{I}^{\mathrm{D}}}(C_{its}^{\mathrm{Drt}}+C_{its}^{\mathrm{LS}})\right]\right\} \tag{12}$$

$$C_{it}^{\mathrm{SU}}=\max\{0,c_i^{\mathrm{u}}(u_{it}-u_{i,t-1})\}\quad\forall i\in\mathcal{I}^{\mathrm{G}},\forall t \tag{13}$$

$$C_{it}^{\mathrm{SD}}=\max\{0,c_i^{\mathrm{d}}(u_{i,t-1}-u_{it})\}\quad\forall i\in\mathcal{I}^{\mathrm{G}},\forall t \tag{14}$$

$$C_{it}^{\mathrm{GR}}=c_{\mathrm{res}}R_{it}^{\mathrm{G}}\quad\forall i\in\mathcal{I}^{\mathrm{G}},\forall t \tag{15}$$

$$C_{it}^{\mathrm{DR}}=c_{\mathrm{res}}R_{it}^{\mathrm{D}}\quad\forall i\in\mathcal{I}^{\mathrm{D}},\forall t \tag{16}$$

$$C_{its}^{\mathrm{OP}}=c_i^0u_{it}+c_i^1p_{its}^{\mathrm{G}}\quad\forall i\in\mathcal{I}^{\mathrm{G}},\forall t,\forall s \tag{17}$$

$$C_{its}^{\mathrm{Grt}}=c_i^1R_{its}^{\mathrm{Grt}}\quad\forall i\in\mathcal{I}^{\mathrm{G}},\forall t,\forall s \tag{18}$$

$$C_{its}^{\mathrm{Drt}}=c_{\mathrm{res}}^{\mathrm{rt}}R_{its}^{\mathrm{Drt}}\quad\forall i\in\mathcal{I}^{\mathrm{D}},\forall t,\forall s \tag{19}$$

$$C_{its}^{\mathrm{LS}}=c_{\mathrm{shed}}(p_{its}^{\mathrm{LS}}+p_{its}^{\mathrm{LSrt}})\quad\forall i\in\mathcal{I}^{\mathrm{D}},\forall t,\forall s \tag{20}$$

where c_i^{u} and c_i^{d} are the startup and shutdown costs of the unit at bus i per time, respectively; c_i^0 and c_i^1 are the linearized generation cost coefficients of the unit at bus i; c_{res} is the day-ahead reserve cost; $c_{\mathrm{res}}^{\mathrm{rt}}$ is the real-time dispatching cost of the demand-side reserve; $\mathcal{I}^{\mathrm{G}}$ and $\mathcal{I}^{\mathrm{D}}$ are the sets of buses equipped with a conventional generator and demand, respectively; u_{it} is the unit status, which (initial state u_{i0}) equals 1 if the unit at bus i and time t is on, and 0 otherwise; R_{it}^{G} is day-ahead scheduled spinning reserve; R_{it}^{D} is the demand-side reserve at bus i and time t; p_{its}^{G} is the output of the unit at bus i and time t in scenario s; p_{its}^{LS} is the scheduled load shedding at bus i and time t in scenario s; and R_{its}^{Grt}, R_{its}^{Drt}, and p_{its}^{LSrt} are the real-time deployed spinning reserve, demand-side reserve, and load shedding at bus i and time t in scenario s, respectively, which are utilized to mitigate the abrupt wind power generation changes.

B. First-stage Constraints

In the first stage, the system operator makes decisions indifferent to the typhoon uncertainties. At bus i, the constraints are as follows:

$$\begin{cases}\sum_{t=1}^{T_i^{\mathrm{O}}}(1-u_{it})=0\\ u_{i0}=1\end{cases}\quad\forall i\in\mathcal{I}^{\mathrm{G}} \tag{21}$$

$$T_i^{\mathrm{U}}(u_{it}-u_{i,t-1})\le\sum_{\tau=t}^{t+T_i^{\mathrm{U}}-1}u_{i\tau}\quad\forall i\in\mathcal{I}^{\mathrm{G}},\forall t=T_i^{\mathrm{O}}+1,T_i^{\mathrm{O}}+2,...,T-T_i^{\mathrm{U}}+1 \tag{22}$$

$$0\le\sum_{\tau=t}^{T}[u_{i\tau}-(u_{it}-u_{i,t-1})]\quad\forall i\in\mathcal{I}^{\mathrm{G}},\forall t=T-T_i^{\mathrm{U}}+2,T-T_i^{\mathrm{U}}+3,...,T \tag{23}$$

$$\begin{cases}\sum_{t=1}^{T_i^{\mathrm{L}}}u_{it}=0\\ u_{i0}=0\end{cases}\quad\forall i\in\mathcal{I}^{\mathrm{G}} \tag{24}$$

$$T_i^{\mathrm{D}}(u_{i,t-1}-u_{it})\le\sum_{\tau=t}^{t+T_i^{\mathrm{D}}-1}(1-u_{i\tau})\quad\forall i\in\mathcal{I}^{\mathrm{G}},\forall t=T_i^{\mathrm{L}}+1,T_i^{\mathrm{L}}+2,...,T-T_i^{\mathrm{D}}+1 \tag{25}$$

$$0\le\sum_{\tau=t}^{T}[1-u_{i\tau}-(u_{i,t-1}-u_{it})]\quad\forall i\in\mathcal{I}^{\mathrm{G}},\forall t=T-T_i^{\mathrm{D}}+2,T-T_i^{\mathrm{D}}+3,...,T \tag{26}$$

$$0\le R_{it}^{\mathrm{G}}\le R_i^{\mathrm{G10m}}u_{it}\quad\forall i\in\mathcal{I}^{\mathrm{G}},\forall t \tag{27}$$

$$0\le R_{it}^{\mathrm{D}}\quad\forall i\in\mathcal{I}^{\mathrm{D}},\forall t \tag{28}$$

where T is the period of the time span; T_i^{U} and T_i^{D} are the minimum uptime and downtime, respectively; T_i^{O} and T_i^{L} are the initial periods when the unit must be online and offline, respectively, which are calculated by $T_i^{\mathrm{O}}=\min\{T,(T_i^{\mathrm{U}}-T_i^{\mathrm{Of}})u_{i0}\}$ and $T_i^{\mathrm{L}}=\min\{T,(T_i^{\mathrm{D}}-T_i^{\mathrm{Lf}})(1-u_{i0})\}$, and T_i^{Of} and T_i^{Lf} are the periods when the unit has been online and offline prior to the first period of the time span, respectively; and R_i^{G10m} is the 10-min ramp rate.

Constraint (21) forces the initial status of the unit at bus i to be on within T_i^{O} periods. In the subsequent periods, the unit has to satisfy the minimum uptime constraints during all the consecutive periods of size T_i^{U} in constraint (22). Constraint (23) ensures that the unit remains on if started in the final $T_i^{\mathrm{U}}-1$ periods. Analogously, the minimum downtime constraints (24)-(26) are identical to (21)-(23) by respective replacement of u_{it}, T_i^{D}, and T_i^{Lf} with $1-u_{it}$, T_i^{U}, and T_i^{Of} [31]. The day-ahead scheduled spinning reserve is limited by a 10-min ramp rate R_i^{G10m} (27), and the demand-side reserve should be non-negative (28).

C. Second-stage Constraints

System operators adjust the output of conventional generators and deploy necessary load shedding adaptively to different typhoon scenarios in the intraday operation. For each scenario s, the second-stage constraints include (the index indicating scenario s is omitted for brevity):

$$p_{it}^{\mathrm{G}}+p_{it}^{\mathrm{W}}+p_{it}^{\mathrm{LS}}-p_{it}^{\mathrm{Lfore}}=\sum_{j\in\mathcal{I}^i}(\theta_{it}-\theta_{jt})/X_{ij}\quad\forall i,\forall t \tag{29}$$

$$-F_{ij}\le(\theta_{it}-\theta_{jt})/X_{ij}\le F_{ij}\quad\forall ij,\forall t \tag{30}$$

$$P_i^{\mathrm{GL}}u_{it}+R_{it}^{\mathrm{G}}\le p_{it}^{\mathrm{G}}\le P_i^{\mathrm{GU}}u_{it}-R_{it}^{\mathrm{G}}\quad\forall i\in\mathcal{I}^{\mathrm{G}},\forall t \tag{31}$$

$$p_{it}^{\mathrm{G}}-p_{i,t-1}^{\mathrm{G}}\le R_i^{\mathrm{GU}}u_{i,t-1}+R_i^{\mathrm{SU}}(u_{it}-u_{i,t-1})\quad\forall i\in\mathcal{I}^{\mathrm{G}},\forall t \tag{32}$$

$$p_{i,t-1}^{\mathrm{G}}-p_{it}^{\mathrm{G}}\le R_i^{\mathrm{GD}}u_{it}+R_i^{\mathrm{SD}}(u_{i,t-1}-u_{it})\quad\forall i\in\mathcal{I}^{\mathrm{G}},\forall t \tag{33}$$

$$0\le p_{it}^{\mathrm{W}}\le p_{it}^{\mathrm{Wfore}}\quad\forall i\in\mathcal{I}^{\mathrm{W}},\forall t \tag{34}$$

$$0\le p_{it}^{\mathrm{LS}}\le p_{it}^{\mathrm{Lfore}}\quad\forall i\in\mathcal{I}^{\mathrm{D}},\forall t \tag{35}$$

where p_{it}^{W} is the output of the wind farm at bus i and time t; θ_{it} is the phase angle at bus i and time t; p_{it}^{Wfore} is the forecasted generation of the wind farm; p_{it}^{Lfore} is the load demand at bus i and time t; $\mathcal{I}^i$ is the set of buses connected to bus i; X_{ij} and F_{ij} are the reactance and capacity of the transmission line ij, respectively; P_i^{GU} and P_i^{GL} are the maximum and minimum outputs, respectively; R_i^{GU} and R_i^{GD} are the ramp-up and ramp-down rates, respectively; $\mathcal{I}^{\mathrm{W}}$ is the set of buses equipped with a wind farm; and R_i^{SU} and R_i^{SD} are the startup and shutdown ramp limits, respectively.

Constraint (29) represents the nodal power balance. Constraint (30) limits the power flow on branch ij. Constraint (31) is the power generation limit. Constraints (32) and (33) denote the ramp-up and ramp-down limits, respectively. Constraint (34) limits the generation of the offshore wind farm, and (35) limits the maximum load shedding. Here, we use the DC power flow model to simplify the UC formulations and take advantage of the tractability of the linear model.

D. Abrupt Wind Power Generation Changes

In practical operation, the fast translation of a typhoon leads to acute wind power generation changes. Figure 6 illustrates the abrupt wind power generation changes of an offshore wind farm affected by a typhoon. This situation may cause an intense wind power ramp-down rate or even shutdown in about 10 min [32].

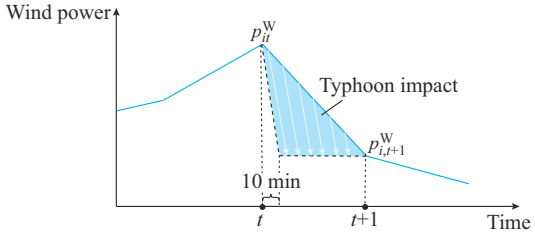

Fig. 6. Abrupt wind power generation changes of an offshore wind farm affected by typhoon.

To relieve these abrupt wind power generation changes, the real-time deployed spinning reserve R_{it}^{Grt}, demand-side reserve R_{it}^{Drt}, and load shedding p_{it}^{LSrt} (real-time dispatching strategy) are utilized. We assume that the wind power generation fluctuates within the range of p_{it}^{W} to $p_{i,t+1}^{\mathrm{W}}$ during $[t,t+1]$ in Fig. 6, and the worst case of the wind power deviation is $\left|p_{it}^{\mathrm{W}}-p_{i,t+1}^{\mathrm{W}}\right|$. When this abrupt wind power generation change causes a power imbalance, the system operator shall adjust the operation of generators, demand response, or even shed the load to recover operational constraints. To guarantee this worst-case feasibility in the real-time dispatching, an adjustable robust optimization framework is adopted [33]. Specifically, for any realization of wind power generation p_{it}^{Wrt} in $[p_{it}^{\mathrm{W}},p_{i,t+1}^{\mathrm{W}}]$, the following constraints are satisfied.

$$p_{it}^{\mathrm{Grt}}+p_{it}^{\mathrm{Wrt}}+p_{it}^{\mathrm{LS}}+p_{it}^{\mathrm{LSrt}}-p_{it}^{\mathrm{Lfore}}+R_{it}^{\mathrm{Drt}}=\sum_{j\in\mathcal{I}^i}(\theta_{it}^{\mathrm{rt}}-\theta_{jt}^{\mathrm{rt}})/X_{ij}\quad\forall i,\forall t \tag{36}$$

$$-F_{ij}\le(\theta_{it}^{\mathrm{rt}}-\theta_{jt}^{\mathrm{rt}})/X_{ij}\le F_{ij}\quad\forall ij,\forall t \tag{37}$$

$$p_{it}^{\mathrm{G}}-R_{it}^{\mathrm{Grt}}\le p_{it}^{\mathrm{Grt}}\le p_{it}^{\mathrm{G}}+R_{it}^{\mathrm{Grt}}\quad\forall i\in\mathcal{I}^{\mathrm{G}},\forall t \tag{38}$$

$$0\le R_{it}^{\mathrm{Grt}}\le R_{it}^{\mathrm{G}}\quad\forall i\in\mathcal{I}^{\mathrm{G}},\forall t \tag{39}$$

$$0\le R_{it}^{\mathrm{Drt}}\le R_{it}^{\mathrm{D}}\quad\forall i\in\mathcal{I}^{\mathrm{D}},\forall t \tag{40}$$

$$p_{it}^{\mathrm{LS}}\le p_{it}^{\mathrm{LS}}+p_{it}^{\mathrm{LSrt}}\le p_{it}^{\mathrm{Lfore}}\quad\forall i\in\mathcal{I}^{\mathrm{D}},\forall t \tag{41}$$

where $\theta_{it}^{\mathrm{rt}}$ is the phase angle at bus i and time t; and p_{it}^{Grt}, R_{it}^{Grt}, R_{it}^{Drt}, and p_{it}^{LSrt} are the adjusted generation, spinning reserve, demand-side reserve, and load shedding, respectively, which are decision variables.

Constraint (36) denotes the nodal power balance. Constraint (37) bounds the power flow on the transmission lines. Constraint (38) ensures that the output of the conventional generator is adjusted with R_{it}^{Grt}. Constraints (39) and (40) ensure that R_{it}^{Grt} and R_{it}^{Drt} are not greater than the day-ahead scheduled reserve. Constraint (41) represents the real-time load shedding limit.

Constraints (36)-(41) are robust against all of the possible wind power generation realizations, and they are difficult to satisfy. However, with offshore wind power curtailment, we can find the worst case lies in the boundary of the box uncertainty set. If the wind power generation is higher than the expectation, no additional risk occurs because the surplus wind power can be curtailed. Therefore, considering wind curtailment, (36) is transformed to:

$$p_{it}^{\mathrm{Grt}}+p_{it}^{\mathrm{Wrt}}+p_{it}^{\mathrm{LS}}+p_{it}^{\mathrm{LSrt}}-p_{it}^{\mathrm{Lfore}}+R_{it}^{\mathrm{Drt}}\ge\sum_{j\in\mathcal{I}^i}(\theta_{it}^{\mathrm{rt}}-\theta_{jt}^{\mathrm{rt}})/X_{ij}\quad\forall i,\forall t,\forall p_{it}^{\mathrm{Wrt}}\in[p_{it}^{\mathrm{W}},p_{i,t+1}^{\mathrm{W}}] \tag{42}$$

The wind power generation p_{it}^{Wrt} is within the box uncertainty set $[p_{it}^{\mathrm{W}},p_{i,t+1}^{\mathrm{W}}]$, so we only need to consider these two boundary values to satisfy (42). When the case $p_{it}^{\mathrm{Wrt}}=p_{it}^{\mathrm{W}}$ is satisfied in the second-stage constraint (29), we only need to consider the wind power generation at time $t+1$:

$$p_{it}^{\mathrm{Grt}}+p_{i,t+1}^{\mathrm{W}}+p_{it}^{\mathrm{LS}}+p_{it}^{\mathrm{LSrt}}-p_{it}^{\mathrm{Lfore}}+R_{it}^{\mathrm{Drt}}\ge\sum_{j\in\mathcal{I}^i}(\theta_{it}^{\mathrm{rt}}-\theta_{jt}^{\mathrm{rt}})/X_{ij}\quad\forall i,\forall t \tag{43}$$

E. Solution Algorithm

For the convenience of discussion, the objective function (12)-(20) is reformulated as (44), and all the constraints (21)-(35), (37) - (41), and (43) are written into a compact form in (45).

$$\min\left(\boldsymbol{c}^{\mathrm{T}}\boldsymbol{x}+\sum_s\boldsymbol{q}_s^{\mathrm{T}}\boldsymbol{y}_s\right) \tag{44}$$

s.t.

$$\boldsymbol{f}(\boldsymbol{x},\boldsymbol{y}_s)\le\boldsymbol{0}\quad\forall s \tag{45}$$

where $\boldsymbol{x}$ denotes the first-stage variables; $\boldsymbol{y}_s$ contains the second-stage variables corresponding to scenario s; and $\boldsymbol{c}$ and $\boldsymbol{q}_s$

are the cost coefficients in the objective function. The overall model is a two-stage MILP problem, which can become computationally intractable when dealing with a large number of typhoon scenarios. To tackle this problem, we adopt the PHA, which has been proven to be an effective algorithm for solving large-scale stochastic mixed-integer programming problems [34], [35]. If the first-stage decision variables $\boldsymbol{x}$ only include binary variables [36], the optimization problem with a squared proximal term can be viewed as an MILP problem. This is because the quadratic term of a binary variable equals the variable itself, i.e., $|\boldsymbol{x}|^2 = x, x \in \{0, 1\}$. However, in our problem, the first-stage variables include the unit status u_{it}, day-ahead scheduled spinning reserve R_{it}^{G}, and demand-side reserve R_{it}^{D}, where the last two terms are continuous variables. Therefore, the PHA involves solving a non-linear mathematical programming problem with the squared proximal term in the objective function, rather than a standard MILP.

In order to mitigate the computational complexity associated with solving mixed-integer quadratic programming (MIQP) in each iteration, we approximate the quadratic terms in the objective function by a linear function, eliminating the need for a quadratic solver. According to [37], the PHA is based on the augmented Lagrangian method, and the L1-norm can be used as the penalty function to achieve an improved convergence speed in the mixed-integer case. Next, we will illustrate how to reformulate an optimization problem into an MILP problem.

Considering the optimization problem in *Step 6* in Algorithm 1, the first three terms are linear functions except for the proximal term $\rho/2\left\|\boldsymbol{x}-\bar{\boldsymbol{x}}^{(k-1)}\right\|_1$ with nonlinearity under Euclidean norm. While under the L1-norm, i.e., the sum of the absolute values of the vector components, the proximal term becomes $\rho/2\left\|\boldsymbol{x}-\bar{\boldsymbol{x}}^{(k-1)}\right\|_1 = \sum_i \rho_i/2\left|x_i-\bar{x}_i^{(k-1)}\right|$ in the following optimization problem.

$$\begin{cases} \min\left(\boldsymbol{c}^{\mathrm{T}}\boldsymbol{x}+\boldsymbol{q}_s^{\mathrm{T}}\boldsymbol{y}_s+\boldsymbol{w}_s^{(k-1)}\boldsymbol{x}+\rho/2\left\|\boldsymbol{x}-\bar{\boldsymbol{x}}^{(k-1)}\right\|_1\right) \\ \text{s.t. } \boldsymbol{f}(\boldsymbol{x},\boldsymbol{y}_s)\le \boldsymbol{0} \quad \forall s \end{cases} \tag{46}$$

where $\boldsymbol{w}_s^{(k-1)}$ is the dual price.

By adding auxiliary variables z_i, the original minimization problem (46) can be written as:

$$\begin{cases} \min\left(\boldsymbol{c}^{\mathrm{T}}\boldsymbol{x}+\boldsymbol{q}_s^{\mathrm{T}}\boldsymbol{y}_s+\boldsymbol{w}_s^{(k-1)}\boldsymbol{x}+\sum_i \rho_i z_i/2\right) \\ \text{s.t. } \boldsymbol{f}(\boldsymbol{x},\boldsymbol{y}_s)\le \boldsymbol{0} \quad \forall s \\ \quad x_i-\bar{x}_i^{(k-1)}\le z_i \\ \quad \bar{x}_i^{(k-1)}-x_i\le z_i \end{cases} \tag{47}$$

The two optimization problems have the same optimal solution based on the following two facts: ① this is a minimization problem; ② we choose parameter ρ in proportion to the generator's output/reserve cost of the associated decision variable, and therefore $\rho > 0$. To sum up, the adopted PHA is summarized in Algorithm 1.

Algorithm 1: PHA

Step 1: initialize iteration number $k=0$

Step 2: for all s, calculate

$$\begin{cases} \boldsymbol{x}_s^{(k)} = \underset{\boldsymbol{x},\boldsymbol{y}_s}{\arg\min}\ \{\boldsymbol{c}^{\mathrm{T}}\boldsymbol{x}+\boldsymbol{q}_s^{\mathrm{T}}\boldsymbol{y}_s\} \\ \text{s.t. } \boldsymbol{f}(\boldsymbol{x},\boldsymbol{y}_s)\le \boldsymbol{0} \quad \forall s \end{cases}$$

Step 3: calculate $\bar{\boldsymbol{x}}^{(k)} = \sum_s \pi_s \boldsymbol{x}_s^{(k)}$

Step 4: for all s, calculate $\boldsymbol{w}_s^{(k)} = \rho(\boldsymbol{x}_s^{(k)} - \bar{\boldsymbol{x}}^{(k)})$

Step 5: update $k = k+1$

Step 6: for all s, calculate

$$\begin{cases} \boldsymbol{x}_s^{(k)} = \underset{\boldsymbol{x},\boldsymbol{y}_s}{\arg\min}\left\{\boldsymbol{q}_s^{\mathrm{T}}\boldsymbol{y}_s+\boldsymbol{w}_s^{(k-1)}\boldsymbol{x}+\rho/2\left\|\boldsymbol{x}-\bar{\boldsymbol{x}}^{(k-1)}\right\|_1\right\} \\ \text{s.t. } \boldsymbol{f}(\boldsymbol{x},\boldsymbol{y}_s)\le \boldsymbol{0} \quad \forall s \end{cases}$$

Step 7: update $\bar{\boldsymbol{x}}^{(k)} = \sum_s \pi_s \boldsymbol{x}_s^{(k)}$

Step 8: for all s, calculate $\boldsymbol{w}_s^{(k)} = \boldsymbol{w}_s^{(k-1)} + \rho(\boldsymbol{x}_s^{(k)} - \bar{\boldsymbol{x}}^{(k)})$

Step 9: if $\sum_s \pi_s\left\|\boldsymbol{x}-\bar{\boldsymbol{x}}^{(k-1)}\right\| \ge \epsilon$ (ϵ is set to be 0.01 in this paper), go to *Step 5*; otherwise, terminate

IV. Case Study

The proposed model is tested for the modified IEEE 30-bus and 118-bus systems. A predefined typhoon moves northwest with an initial location at (123.3°E, 23.1°N), as shown in Fig. 7.

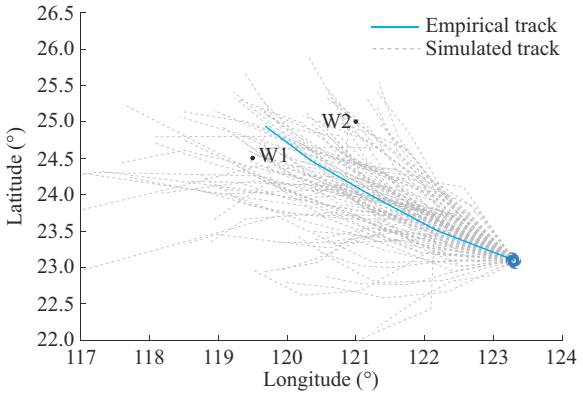

Fig. 7. Typhoon track simulation.

As mentioned, the accumulation of prediction errors in the translation speed and heading direction of a typhoon track leads to increased uncertainties in the typhoon track forecast. While obtaining an accurate typhoon track from a few hours ago is challenging, updating the latest typhoon information allows us to incorporate more up-to-date information and obtain a less conservative solution for the optimization problem. We generate 100 samples of typhoon track scenarios. Of these, 50 scenarios are used for stochastic UC optimization, and the other 50 are real-world scenarios for validation. Two offshore wind farms are located at (120°E, 25°N) and (123°E, 24.3°N). The stochastic UC model is modeled using the YALMIP package [38] and solved by Gurobi [39] in MATLAB R2016. To validate the proposed method, we compare its performance in the following four cases: ① Case 1: scenario-based UC considering the anti-typhoon mode; ② Case 2: deterministic UC considering the anti-typhoon

mode; ③ Case 3: scenario-based UC considering the anti-typhoon mode but regardless of the abrupt wind power generation changes; ④ Case 4: scenario-based UC ignoring the anti-typhoon mode.

A. Modified IEEE 30-bus System

The test system is equipped with two offshore wind farms at buses 1 and 22 (W1 and W2) [40]. Their installed capacities are 40 and 60 MW, respectively. The system net load is based on that in [41], and the generator data are modified from [42].

Along the empirical typhoon track, the forecasted wind power generation of two offshore wind farms considering the anti-typhoon mode is shown in Fig. 8.

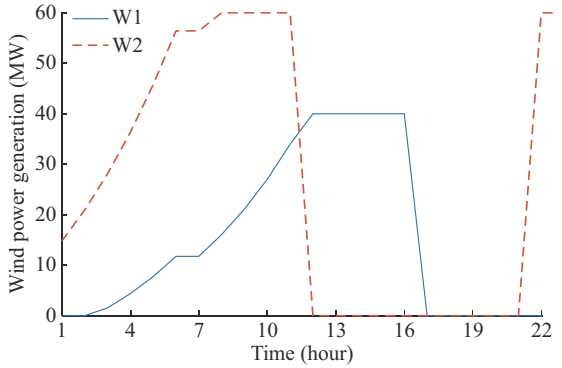

Fig. 8. Forecasted wind power generation of two offshore wind farms considering anti-typhoon mode.

When the anti-typhoon mode is ignored, the wind power generation is changed to that shown in Fig. 9. Case 2 adopts the deterministic wind power generation profiles in Fig. 8, while the other cases adopt wind power generation profiles corresponding to the 50 simulated typhoon tracks. The UC strategies of different cases are displayed in Fig. 10.

1) Optimality of Different Cases

To test the average costs of different cases in multiple scenarios, we fix the first-stage variables $\boldsymbol{x}$ (unit status, day-ahead spinning reserve, and demand-side reserve) of each case, and the scenarios in all cases are set to be the 50 simulated typhoon scenarios. Then, we solve the resultant optimization problem given by (44) and (45) and obtain the average costs of different cases, which are summarized in Table I. In general, the average operational cost increases gradually from Case 1 to Case 4. The average load shedding and average wind curtailment in different cases during different hours are presented in Figs. 11 and 12, respectively. The average load shedding is more significant during hours 14 to 18 when the offshore wind farms are likely to be cut off due to the anti-typhoon mode. Case 1 shows slightly less wind curtailment than other cases.

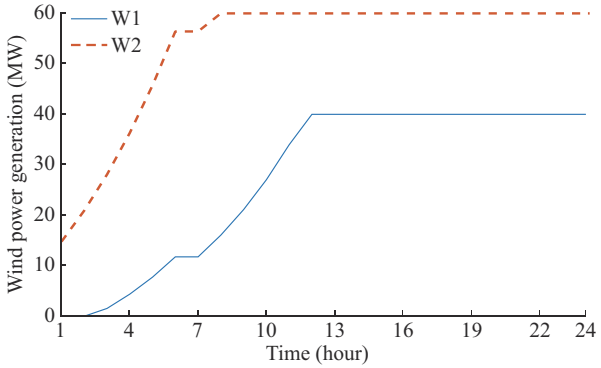

Fig. 9. Forecasted wind power generation of two offshore wind farms ignoring anti-typhoon mode.

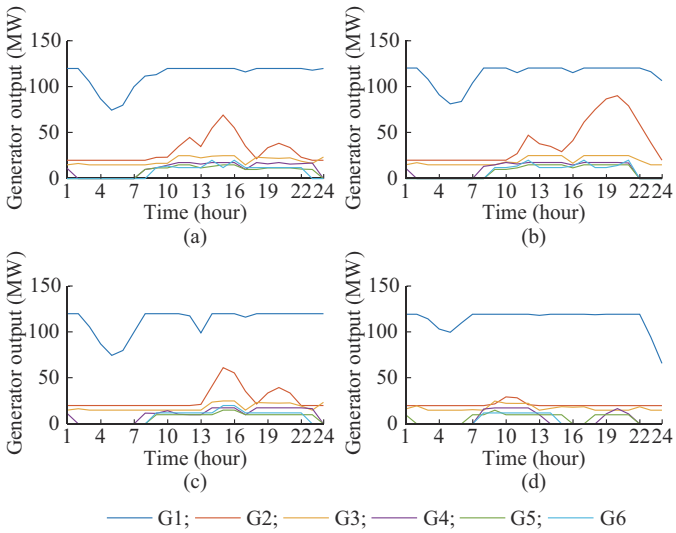

Fig. 10. UC strategies of different cases. (a) Case 1. (b) Case 2. (c) Case 3. (d) Case 4.

TABLE I
OPERATIONAL COSTS OF DIFFERENT CASES UNDER 50 TYPHOON SCENARIOS IN IEEE 30-BUS SYSTEM

Case	Total cost (k$)	Generator start-up/shutdown cost (k$)	Generator reserve (k$)	Demand-side reserve (k$)	Generator operating cost (k$)	Real-time deployed spinning reserve (k$)	Real-time demand-side reserve (k$)	Load shedding cost (k$)
Case 1	123.4	0.1	1.0	1.8	118.0	1.0	1.5	0.1
Case 2	127.6	0.1	0.5	0.9	122.9	0.6	1.0	1.8
Case 3	131.8	0.1	0	0	123.4	0	0	8.4
Case 4	136.4	0.1	0	0	123.3	0	0	13.0

2) Comparing Stochastic UC with Deterministic One

The stochastic UC of Case 1 has more "on" status units during hours 22 to 23 than the deterministic one of Case 2, as shown in Fig. 10(a) and (b). The forecasted errors of empirical tracks increase over time while these stochastic tracks can be better described by different typhoon scenarios. The stochastic UC outperforms the deterministic one with a lower cost and less load shedding by preparing more generator and demand-side reserve, as shown in Table I.

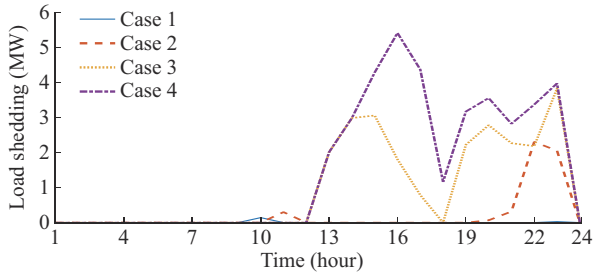

Fig. 11. Average load shedding in different cases.

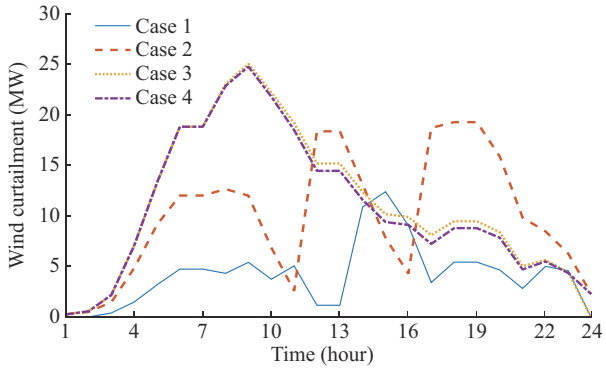

Fig. 12. Average wind curtailment in different cases.

3) Influence of Abrupt Wind Power Generation Changes

The unit statuses when considering or ignoring abrupt wind power generation changes are almost the same, as shown in Fig. 10(a) and (c). Case 1 considers the abrupt wind power generation changes and entails a wider range of generator adjustments. Therefore, it prepares a greater day-ahead spinning reserve and demand-side reserve and reduces the operational costs and load shedding compared with Case 3. Because day-ahead reserves merely relieve operational risks caused by fast typhoon track, regardless of these risks, Case 3 prepares no reserves.

4) Influence of Considering Anti-typhoon Mode

Case 1, which considers the anti-typhoon mode, deploys more units during hours 14 to 18 than Case 4. Case 1 significantly reduces the load shedding, given that offshore wind farms are likely to be cut off under high wind speeds during this time. However, neglecting it in Case 4 results in high load shedding, as shown in Fig. 11.

5) Sensitivity Analysis of Wind Penetration Rate

The proposed model is tested with the wind penetration rate rising from 10% to 60%, as shown in Fig. 13. The installed capacities of W1 and W2 are modified to $115p$ and $172.5p$ MW, respectively, under penetration rate p. In the scenario of low penetration rate, the operational costs of different cases are similar, mainly composed of the operational costs of the thermal generators. Under a scenario of higher penetration rate, Case 1 reduces the total cost, while the other cases increase the total costs significantly due to massive load shedding. This is because Case 1 purchases more reserves and considers the operating features of offshore wind farms under typhoon impacts. The operation strategy of Case 4, which ignores the anti-typhoon mode, is too optimistic about wind power generation, resulting in the highest load shedding under a high penetration rate.

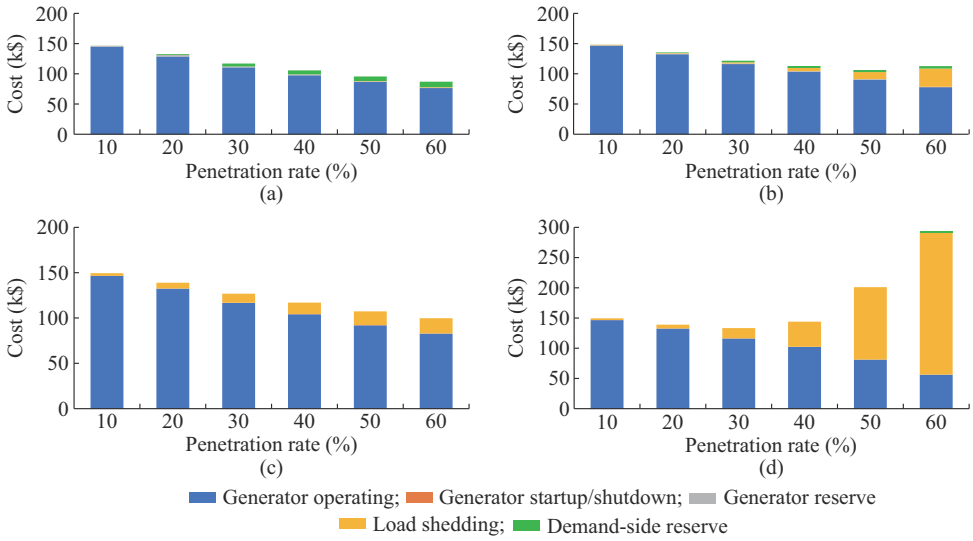

Fig. 13. Operational costs of different cases under various wind penetration rates in IEEE 30-bus system. (a) Case 1. (b) Case 2. (c) Case 3. (d) Case 4.

6) Sensitivity Analysis of Numbers of Scenarios

We compare the computation time and optimal objective function value of the stochastic UC model in terms of different numbers of scenarios, as shown in Figs. 14 and 15. Total 200 scenarios are generated by the Monte Carlo sampling. To test the performance of scenario s in the experiments, we randomly select s scenarios from 200 scenarios, repeat solving the stochastic models ten times, and calculate the average optimal value and computation time. As the number of scenarios gradually rises from 20 to 200, we find that the computation time increases rapidly with the number of scenarios, but the optimal value remains stable with slight fluctuations after 40 scenarios (the expected deviation of the optimal value is less than 0.3%). Therefore, we can choose 50 scenarios to achieve a good optimal value with a relatively low computational burden.

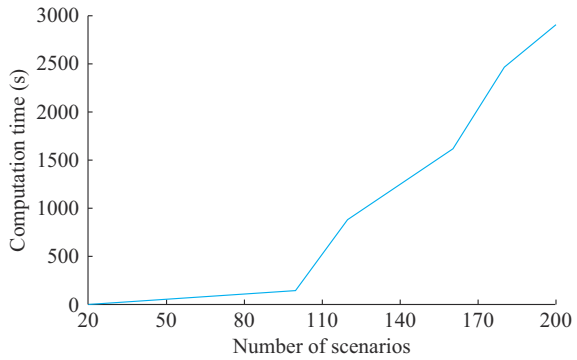

Fig. 14. Computation time of stochastic UC model in terms of different numbers of scenarios.

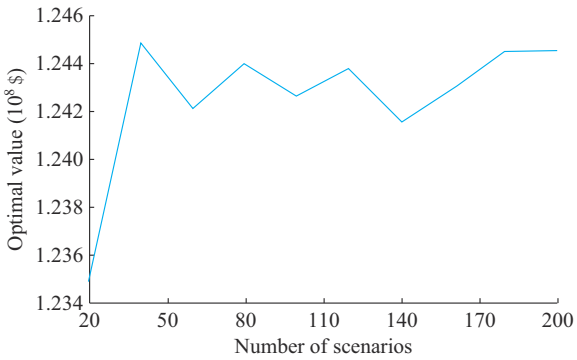

Fig. 15. Optimal objective function values of stochastic UC model in terms of different numbers of scenarios.

B. Modified IEEE 118-bus System

1) Optimality of Different Cases

The test system is equipped with two wind farms at buses 49 and 70, both with capacities of 1255 MW modified from [43].

Similar to the IEEE 30-bus system, we test the average costs of different cases in 50 simulated typhoon scenarios, as shown in Table II. Case 1 outperforms the other cases with a lower total operational cost and less load shedding. Ignoring anti-typhoon mode causes the most severe load shedding in Case 4.

TABLE II
OPERATIONAL COSTS OF DIFFERENT CASES IN 50 TYPHOON SCENARIOS IN IEEE 118-BUS SYSTEM

Case	Total cost (k$)	Generator startup/ shutdown cost (k$)	Generator reserve (k$)	Demand-side reserve (k$)	Generator operating cost (k$)	Real-time deployed spinning reserve (k$)	Real-time demand-side reserve (k$)	Load shedding cost (k$)
Case 1	2334.2	2.3	12.4	2.6	2059.4	19.5	3.7	234.3
Case 2	2475.9	2.3	16.7	2.5	2026.1	27.6	3.3	397.4
Case 3	2384.5	1.9	0	0	2043.1	0	0	339.6
Case 4	3232.0	1.9	1.8	0	1979.0	0.2	0	1249.1

2) Sensitivity Analysis of Wind Penetration Rate

The sensitivity analysis results with the wind penetration rate varying from 10% to 60% in the IEEE 118-bus system are shown in Fig. 16. The installed capacities of the conventional generators are fixed, and the offshore wind farm capacities are adjusted based on the penetration rate. As the penetration rate grows, the power generation of the conventional generators gradually decreases. Case 1 reduces the load shedding and obtains a lower total operational cost than the other cases.

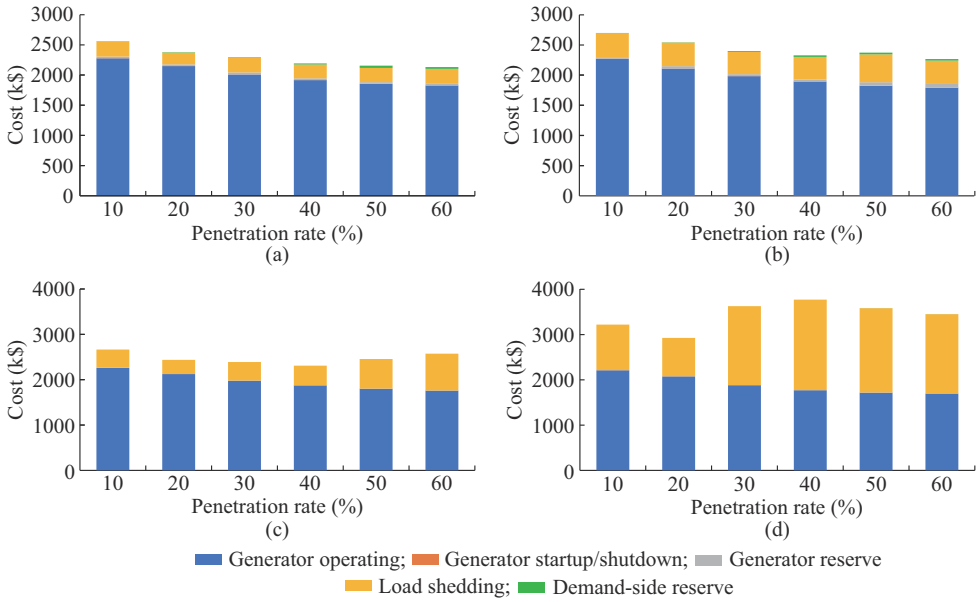

Fig. 16. Operational costs of different cases under various penetration rates in IEEE 118-bus system. (a) Case 1. (b) Case 2. (c) Case 3. (d) Case 4.

3) Computational Efficiency

The computation time and optimal objective function values when different algorithms are used to solve the two-stage MILP problem are displayed in Table III. The centralized algorithm, i.e., directly solving (44) and (45), obtains a global optimal solution, but it requires a massive solution time with the growth of the number of scenarios. Specifically, the centralized algorithm fails to solve the 50-scenario problem (N/A in Table III) in 5 hours. The PHA in Algorithm 1 compromises optimality and efficiency to obtain a near optimal solution. In comparison to the centralized algorithm, the relative error of the optimal solution obtained by the PHA is less than 2% in the IEEE 30-bus system and 6% in the IEEE 118-bus system.

TABLE III
COMPUTATION TIME AND OPTIMAL OBJECTIVE FUNCTION VALUES OF DIFFERENT ALGORITHMS FOR DIFFERENT NUMBERS OF SCENARIOS

Case	Number of scenarios	Centralized algorithm		PHA	
		Objective (k$)	Time (s)	Objective (k$)	Time (s)
IEEE 30-bus	25	123.6	17.6	125.3	35.5
	50	123.4	51.7	125.0	71.8
	100	123.0	159.7	124.8	150.9
IEEE 118-bus	25	2205.7	1611.8	2338.8	328.9
	50	N/A	18000.0	2334.2	624.0
	100	N/A	18000.0	2312.3	1454.7

V. CONCLUSION

Offshore wind has excellent prospects in the future. Nevertheless, wind farms are susceptible to extreme weather such as typhoons along the South China coast. To describe the spatial-temporal impacts of typhoons, we consider the time-varying wind field and utilize an empirical track model. To account for the uncertainties associated with typhoon tracks, we employ a data-driven method to generate multiple scenarios for an upcoming typhoon. Recognizing the significant influence of typhoons on offshore wind farms, the anti-typhoon mode and the abrupt wind power generation changes in the intra-hour interval are taken into account. A two-stage stochastic UC is proposed to minimize the operational costs and load shedding under typhoon uncertainties. To tackle the computational burden associated with solving the stochastic UC problem, we employ the PHA. Simulation results show that considering the anti-typhoon mode and the abrupt wind power generation change is beneficial for reducing the total operational costs and load shedding.

In the future, we would expand our work on model improvement and new method application. For model improvement, we would consider the power system cooperating with other systems, e.g., the district heating system, to enhance resilience. Demand response, distributed generation units, and other resources are scheduled to resist typhoons. Furthermore, the complex variations of the power system model in typhoon scenarios can be considered, such as destructions in components and changes in topology. For new method application, the integration of emerging artificial intelligence technologies like deep neural networks and reinforcement learning is promising to achieve higher computational efficiency and enforce safety operations.

REFERENCES

[1] M. Li, E. Virguez, R. Shan *et al*., "High-resolution data shows China's wind and solar energy resources are enough to support a 2050 decarbonized electricity system," *Applied Energy*, vol. 306, p. 117996, Jan. 2022.

[2] X. Liu, T. Zhao, C.-T. Chang *et al*., "China's renewable energy strategy and industrial adjustment policy," *Renewable Energy*, vol. 170, pp. 1382-1395, Jun. 2021.

[3] Y. Li, X. Qiao, C. Chen *et al*., "Integrated optimal siting and sizing for VSC-HVDC-link-based offshore wind farms and shunt capacitors," *Journal of Modern Power Systems and Clean Energy*, vol. 9, no. 2, pp. 274-284, Mar. 2021.

[4] A. Akrami, M. Doostizadeh, and F. Aminifar, "Power system flexibility: an overview of emergence to evolution," *Journal of Modern Power Systems and Clean Energy*, vol. 7, no. 6, pp. 987-1007, Sept. 2019.

[5] N. Yang, Z. Dong, L. Wu *et al*., "A comprehensive review of security-constrained unit commitment," *Journal of Modern Power Systems and Clean Energy*, vol. 10, no. 3, pp. 562-576, May 2022.

[6] X. Zhu, Z. Yu, and X. Liu, "Security constrained unit commitment with extreme wind scenarios," *Journal of Modern Power Systems and Clean Energy*, vol. 8, no. 3, pp. 464-472, May 2020.

[7] "Robust unit commitment problem with demand response and wind energy," in *Proceedings of 2012 IEEE PES General Meeting*, San Diego, USA, Nov. 2012, pp. 1-8.

[8] Y. Yang, W. Wu, B. Wang *et al*., "Analytical reformulation for stochastic unit commitment considering wind power uncertainty with Gaussian mixture model," *IEEE Transactions on Power Systems*, vol. 35, no. 4, pp. 2769-2782, Jul. 2019.

[9] P. Sherman, X. Chen, and M. McElroy, "Offshore wind: an opportunity for cost-competitive decarbonization of China's energy economy," *Science Advances*, vol. 6, p. eaax9571, Feb. 2020.

[10] S. Yuan, S. M. Quiring, L. Zhu *et al*., "Development of a typhoon power outage model in Guangdong, China," *International Journal of Electrical Power and Energy Systems*, vol. 117, p. 105711, May 2020.

[11] Y. Sang, J. Xue, M. Sahraei-Ardakani *et al*., "An integrated preventive operation framework for power systems during hurricanes," *IEEE Systems Journal*, vol. 14, pp. 3245-3255, Sept. 2020.

[12] S. Ma, B. Chen, and Z. Wang, "Resilience enhancement strategy for distribution systems under extreme weather events," *IEEE Transactions on Smart Grid*, vol. 9, no. 2, pp. 1442-1451, Mar. 2018.

[13] O. Hajimiri, A. Rabiee, S. M. Mohseni-Bonab *et al*., "Resilience-constrained unit commitment considering demand response," in *Proceedings of 2021 IEEE PES General Meeting*, Washington DC, USA, Jul. 2021, pp. 1-5.

[14] Y. Wang, L. Huang, M. Shahidehpour *et al*., "Resilience-constrained hourly unit commitment in electricity grids," *IEEE Transactions on Power Systems*, vol. 33, no. 5, pp. 5604-5614, Sept. 2018.

[15] D. N. Trakas and N. D. Hatziargyriou, "Resilience constrained day-ahead unit commitment under extreme weather events," *IEEE Transactions on Power Systems*, vol. 35, no. 2, pp. 1242-1253, Mar. 2020.

[16] J. Li, Z. Li, Y. Jiang *et al*., "Typhoon resistance analysis of offshore wind turbines: a review," *Atmosphere*, vol. 13, p. 451, Mar. 2022.

[17] Q. Wang, Z. Yu, R. Ye *et al*., "An ordered curtailment strategy for offshore wind power under extreme weather conditions considering the resilience of the grid," *IEEE Access*, vol. 7, pp. 54824-54833, Apr. 2019.

[18] W. Yuan, J. Wang, F. Qiu *et al*., "Robust optimization-based resilient distribution network planning against natural disasters," *IEEE Transactions on Smart Grid*, vol. 7, no. 6, pp. 2817-2826, Nov. 2016.

[19] R.-P. Liu, S. Lei, C. Peng *et al*., "Data-based resilience enhancement strategies for electric-gas systems against sequential extreme weather events," *IEEE Transactions on Smart Grid*, vol. 11, no. 6, pp. 5383-5395, Nov. 2020.

[20] G. Li, P. Zhang, P. B. Luh *et al*., "Risk analysis for distribution systems in the northeast US under wind storms," *IEEE Transactions on Power Systems*, vol. 29, no. 2, pp. 889-898, Mar. 2014.

[21] P. J. Vickery, F. J. Masters, M. D. Powell *et al*., "Hurricane hazard modeling: the past, present, and future," *Journal of Wind Engineering and Industrial Aerodynamics*, vol. 97, pp. 392-405, Sept. 2009.

[22] D. Liu, L. Pang, and B. Xie, "Typhoon disaster in China: prediction, prevention, and mitigation," *Natural Hazards*, vol. 49, pp. 421-436, Mar. 2009.

[23] P. Vickery, P. Skerlj, and L. Twisdale, "Simulation of hurricane risk in the US using empirical track model," *Journal of Structural Engineering*, vol. 126, pp. 1222-1237, Oct. 2000.
[24] H. Zhang, L. Cheng, S. Yao *et al*., "Spatial-temporal reliability and damage assessment of transmission networks under hurricanes," *IEEE Transactions on Smart Grid*, vol. 11, no. 2, pp. 1044-1054, Mar. 2020.
[25] Q. Zheng, J. Wang, and A. Liu, "Stochastic optimization for unit commitment: a review," *IEEE Transactions on Power Systems*, vol. 30, no. 4, pp. 1913-1924, Jul. 2015.
[26] Y. Wang and D. V. Rosowsky, "Joint distribution model for prediction of hurricane wind speed and size," *Structural Safety*, vol. 35, pp. 40-51, Mar. 2012.
[27] CMA Tropical Cyclone Data Center (2023, Mar.). Typhoon path data set. [Online]. Available: https://tcdata.typhoon.org.cn/zjljsjjsm.html
[28] A. Shapiro and T. Homem-de-Mello, "On the rate of convergence of optimal solutions of Monte Carlo approximations of stochastic programs," *SIAM Journal on Optimization*, vol. 11, no. 1, pp. 70-86, Oct. 1999.
[29] A. Shapiro and A. Nemirovski, "On complexity of stochastic programming problems," *Continuous Optimization*, vol. 99, pp. 111-146, Apr. 2005.
[30] P. Javanbakht and S. Mohagheghi, "A risk-averse security-constrained optimal power flow for a power grid subject to hurricanes," *Electric Power Systems Research*, vol. 116, pp. 408-418, Nov. 2014.
[31] M. Carrión and J. M. Arroyo, "A computationally efficient mixed-integer linear formulation for the thermal unit commitment problem," *IEEE Transactions on Power Systems*, vol. 21, no. 3, pp. 1371-1378, Aug. 2006.
[32] Y.-H. Kim, J. Kim, Y. Kang *et al*., "Shutdown of an offshore wind power plant without using a brake to meet the required ramp rate in various storm-driven conditions," *Energy*, vol. 82, pp. 1011-1020, Mar. 2015.
[33] W. Wei, F. Liu, S. Mei *et al*., "Robust energy and reserve dispatch under variable renewable generation," *IEEE Transactions on Smart Grid*, vol. 6, no. 1, pp. 369-380, Jan. 2015.
[34] J.-P. Watson and D. L. Woodruff, "Progressive hedging innovations for a class of stochastic mixed-integer resource allocation problems," *Computational Management Science*, vol. 8, pp. 355-370, Aug. 2011.
[35] W. Zhang, B. Hu, K. Xie *et al.*, "Short-term transmission maintenance scheduling considering network topology optimization," *Journal of Modern Power Systems and Clean Energy*, vol. 10, no. 4, pp. 883-893, Jul. 2022.
[36] S. M. Ryan, R. J.-B. Wets, D. L. Woodruff *et al*., "Toward scalable, parallel progressive hedging for stochastic unit commitment," in *Proceedings of 2013 IEEE PES General Meeting*, Vancouver, Canada, Nov. 2013, pp. 1-5.
[37] V. Kaisermayer, D. Muschick, M. Horn *et al*., "Progressive hedging for stochastic energy management systems," *Energy Systems*, vol. 12, pp. 1-29, Aug. 2021.
[38] J. Lofberg, "Yalmip: a toolbox for modeling and optimization in MATLAB," in *Proceedings of 2004 IEEE International Conference on Robotics and Automation*, Taipei, China, Sept. 2004, pp. 284-289.
[39] Gurobi Optimization. (2021, Aug.). Gurobi optimizer reference manual. [EB/OL]. Available: https://www.gurobi.com/documentation/9.1/refman/index.html
[40] Y. Liu, Z. Li, Q. Wu *et al*., "Real-time dispatchable region of renewable generation constrained by reactive power and voltage profiles in AC power networks," *CSEE Journal of Power and Energy Systems*, vol. 6, no. 5, pp. 528-536, Sept. 2020.
[41] Illinois Institute of Technology. (2015, Jul.). RSCUC 118 UMP. [Online]. Available: http://motor.ece.iit.edu/data/
[42] Z. Li, L. Li, Y. Wang *et al*., "Mixed-integer linear programming model and constraints reduction methods for security-constrained unit commitment," in *Proceedings of 2020 IEEE Sustainable Power and Energy Conference*, Chengdu, China, Nov. 2020, pp. 1437-1443.
[43] Y. Liu, Z. Li, W. Wei *et al*., "Data-driven dispatchable regions with potentially active boundaries for renewable power generation: concept and construction," *IEEE Transactions on Sustainable Energy*, vol. 13, no. 2, pp. 882-891, Apr. 2022.

Yanqi Liu received the B.S. and M.S. degrees from the School of Electric Power Engineering, South China University of Technology, Guangzhou, China. He is currently pursuing a Ph.D. degree at the University of Macau, Macao, China. His research interests include resilience assessment, renewable energy, and integrated energy systems planning and operation.

Dundun Liu received the Ph. D. degree in electrical engineering from Shanghai Jiao Tong University, Shanghai, China, in 2021. He is currently working as an Associate Researcher with University of Macau Zhuhai UM Science and Technology Research Institute, Zhuhai, China. His research interests include power system planning and security analysis.

Hongcai Zhang received the B.S. and Ph.D. degrees in electrical engineering from Tsinghua University, Beijing, China, in 2013 and 2018, respectively. He is currently an Assistant Professor with the State Key Laboratory of Internet of Things for Smart City and Department of Electrical and Computer Engineering, University of Macau, Macao, China. From 2018-2019, he was a Postdoctoral Scholar with the Energy, Controls, and Applications Lab, University of California, Berkeley, USA, where he was a Visiting Student Researcher in 2016. His current research interests include Internet of Things for smart energy, optimal operation and optimization of power and transportation systems, and grid integration of distributed energy resources.